Rotating-field magnetoresistance of exchange-biased spin valves

Amitesh Paul,[a] Matthias Buchmeier, Daniel E. Bürgler, and Peter Grünberg
Institut für Festkörperforschung, Forschungszentrum, Jülich GmbH, D-52425 Jülich, Germany

(Received 9 August 2004; accepted 2 November 2004; published online 27 December 2004)

We investigate the magnetoresistance (MR) of spin valves by (i) varying the strength of the field applied in a fixed direction and (ii) rotating the field with fixed strength. The latter data reflect in general a mixture of giant and anisotropic magnetoresistance (GMR and AMR). We present an experimental procedure to suppress the AMR contributions of all ferromagnetic layers in the spin valve without disturbing the GMR response. The resulting angular MR curves are fitted with a single-domain model to determine with high precision the exchange bias field, the uniaxial anisotropies, the GMR ratio, and the interlayer coupling field. The application of the method to differently prepared Ta(5.0 nm)/NiFe(3.0 nm)/FeMn(15.5 nm)/NiFe(3.0 nm)/Co(2.0 nm)/Cu(3.5 nm)/Co(2.0 nm)/NiFe(7.0 nm) spin valves with GMR ratios of 1.8% and 4% demonstrates the sensitivity and reveals differences of the order of a few percents of the exchange bias field for the uniaxial anisotropy fields of the free and pinned layer as well as for the interlayer coupling field. © *2005 American Institute of Physics*. [DOI: 10.1063/1.1836881]

I. INTRODUCTION

A standard spin-valve structure consists of two ferromagnetic (FM) layers separated by a nonmagnetic (noble) metal spacer, where one of the FM layers, the so-called reference of fixed layer, is pinned by an antiferromagnetic (AF) layer[1] due to the exchange bias[2] effect arising from direct exchange coupling at the FM/AF interface. The exchange bias acts as a unidirectional anisotropy and thus "locks" the magnetization of the pinned FM in a certain direction, even for external fields applied in the opposite direction if they are lower than the exchange bias field $|H_{EB}|$.[3,4] In contrast, the other FM layer of the spin valve, the so-called sensor or free layer, should freely follow the external field and, therefore, is chosen to be magnetically soft. Magnetic sensors based on the giant magnetoresistance (GMR)[5,6] in spin-valve structures require a low coercive field of the free layer and a large H_{EB} of the fixed layer in order to yield a well-defined response over a wide range of field strength and direction.

The magnetoresistive output of a spin valve when exposed to an external field varying in magnitude and/or direction depends sensitively on the details of the remagnetization process, which is influenced by the anisotropies and coercivities of the FM layers, their anisotropic magnetoresistance (AMR), the unidirectional exchange bias anisotropy of the pinned layer, and eventually the magnetic coupling between the two FM layers.

AMR measurements as a function of the applied field direction have previously been applied to AF/FM bilayer to determine H_{EB}[7] and to map the distribution of exchange bias directions.[8] Here, we study the dependence of the magnetoresistance (MR) on the field direction in spin-valve structures instead of bilayers in order to take advantage of the GMR, which yields a higher sensitivity. Moreover, spin valves have a higher relevance for practical applications. Additionally, we will present an experimental procedure to suppress all AMR contributions which allows us to determine with high precision the parameters relevant for the exchange bias effect and the GMR response.[9]

We choose the FeMn/NiFe exchange bias system for the following reasons: (i) low coercivity of NiFe, (ii) high Néel temperature T_N=458 K of FeMn above room temperature (RT), (iii) sizable H_{EB}, and (iv) simple, nonreactive sputter process. The system has intensively been studied in order to optimize H_{EB} and to explore the relation between magnetic properties, microstructure, and interface roughness.[10–14]

II. EXPERIMENT

The spin valves are prepared by dc magnetron sputtering in a system with a base pressure of 10^{-7} mbar. The layer sequence grown on oxidized Si substrates is Ta(5.0 nm)/NiFe(3.0 nm)/FeMn(15.5 nm)/NiFe(3.0 nm)/Co(2.0 nm)/Cu(3.5 nm)/Co(2.0 nm)/NiFe(7.0 nm) (see Fig. 1). A Ta underlayer serves as a buffer, and the NiFe texturing layer provides a (111) texture[12] for the FeMn layer. The NiFe film on top of AF FeMn layer together with a thin Co polarizing layer represent the fixed layer of the spin valve. A Cu spacer separates it from the free layer which also consists of a Co polarizing layer and NiFe. Polarizing Co layers on both sides of the spacer enhance the GMR ratio due to the higher degree of spin polarization of Co (≈42%) compared to NiFe (≈35%).[15]

We prepare two types of spin valves labeled S1 and S2, for which the field-cooling procedure is performed at different stages of the deposition sequence. Therefore, we expect different magnetic and magnetotransport properties. The field-cooling procedure consists of annealing in an inert atmosphere of N_2 gas for 10 min at 473 K, i.e., above the Néel temperature T_N=458 K of FeMn, and subsequently cooling to RT in an applied field of 130 Oe. For type S1 the annealing is performed before the growth of the free layer. In this case a field of 130 Oe is applied during the growth of the

[a]Author to whom correspondence should be addressed; electronic mail: a.paul@fz-juelich.de

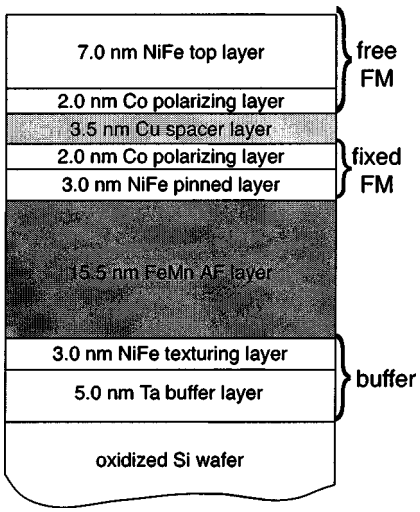

FIG. 1. Schematic sequence of the spin-valve structure. The fixed and free FM layers consist of a NiFe layer and a Co polarizing layer at the interface towards the Cu spacer.

free FM layer. Type S2 spin valves are annealed after completion of the whole sequence. The resulting slightly different magnetic properties can be extracted from angular MR measurements, but not from standard MR and magneto-optical Kerr effect (MOKE) measurements.

The main characterization tool of this work is the measurement of the MR as a function of the field magnitude as well as the field direction. We employ a conventional four-probe dc technique with the applied constant current flowing parallel to the easy axis of the pinned layer, i.e., the direction of magnetic field during the field-cooling procedure. Unpatterned square or rectangular samples of about 1 cm^2 size are contacted using needles or wire bonding. We used different contact geometries that will be defined and discussed in Sec. IV. MR measurements are performed with two types of setups: In setup I we vary the strength and sign of the external field applied in a fixed direction collinear to the exchange bias direction (EBD), and in setup II we rotate the external field with a fixed magnitude.[16,17] In the latter case we employ a pair of permanent magnets and vary the field strength from 30 to 600 Oe by adjusting the separation of the permanent magnets. The magnetic field is applied in the plane of the sample for all measurements. The GMR ratio is defined in the usual manner as $(R_0-R_S)/R_S$, where R_S and R_0 are the resistances at saturating and zero magnetic field, respectively.

Magnetization loops are recorded by means of the MOKE at RT in setup I. Atomic force microscopy (AFM) measurements are performed in the tapping mode using a multimode scanning probe microscope from Digital Instruments. X-ray reflectivity (XRR) as well as diffuse x-ray scattering (XDS) measurements[18,19] are employed to characterize the microstructure of the samples. We use a Bruker-axs D8 diffractometer with Cu $K\alpha$ radiation. XRR measurements are done in specular geometry, where the angle of incidence α_i equals the angle of reflection α_r. Diffuse scattering as a function of the in-plane component of the momentum transfer vector q_x is measured by keeping the scattering angle 2α fixed while rocking the specimen around $\alpha_i=\alpha_r$.

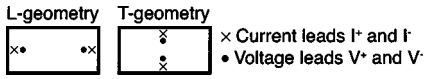

FIG. 2. Contact configuration of the four-probe resistance measurements: longitudinal (L geometry) and transverse (T geometry).

III. MODEL

In order to qualitatively analyze the angular MR data, we model the magnetic state of the system in a single-domain approach assuming rigid in-plane magnetizations.[20] The equilibrium magnetization angles $\theta_{f,p,\ldots}$ of the free, pinned, and possible additional FM layers at a given external field H applied at angle θ with respect to the EBD are calculated numerically from the total minima of the free energy per unit area. In our case, the NiFe texturing layer is an additional FM that also contributes via AMR to the total MR response. Another example for the occurrence of additional FM layers that need to be considered are spin valves with an artificial antiferromagnet.[21] For the free energy expression, we take into account the Zeeman energies and the uniaxial anisotropies of all FM layers (anisotropy constants $Ku_{f,p,\ldots}$ for free, pinned, and additional FM layers, respectively), bilinear interlayer coupling between the free and pinned layer parametrized by J, and the unidirectional anisotropy of the pinned layer given by H_{EB}.

The total MR due to both GMR and AMR is then calculated from the equilibrium configuration at a given external field by

$$R = R_0 + \Delta R_{GMR}\frac{1}{2}\{1-\cos(\theta_f-\theta_p)\} + \sum_{i=f,p,\ldots}\Delta R_{AMR,i}\sin^2(\theta_i-\theta_I), \quad (1)$$

where R_0 is the field-independent resistance, ΔR_{GMR} the GMR amplitude, θ_I the direction of the current, and θ_i and $\Delta R_{AMR,i}$ $(i=f,p,\ldots)$ denote the magnetization directions and the AMR amplitudes of the FM layers.

IV. INFLUENCE OF CONTACT GEOMETRY ON AMR

We use different contact geometries labeled "L" for longitudinal and "T" for transverse geometry as shown in Fig. 2. Typical linear dimensions of the samples are of the order of 10 mm. The contact geometry has a strong influence on the current distribution in the sample. The GMR effect depends on the relative angle $\theta_f-\theta_p$ between the free and pinned layer and is for isotropic polycrystalline samples independent of the in-plane current direction. Therefore, the measured GMR ratio is not expected to be affected by the contact geometry. On the other hand, the macroscopically measured AMR ratio is expected to strongly depend on the current distribution in the sample, because AMR depends on the angle between the local magnetization and the current direction. The AMR ratio measured for a homogeneous current distribution reflects in good approximation the microscopic AMR ratio. For current distributions where the current pre-

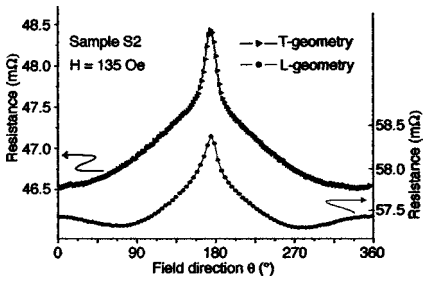

FIG. 3. Angular dependence of the resistance R for sample S2 measured at 135 Oe in transverse (T) and longitudinal (L) contact geometry. The ordinates are equally scaled but offset by about 11 mΩ.

dominantly flows along circular trajectories, local AMR contributions average out, and the macroscopically measured AMR ratio is strongly reduced.

As an example we show in Fig. 3 the angular MR of sample S2 measured at the same field strength of 135 Oe in the two different contact geometries. The curves show a distinctly diverse course, because the AMR of the three (free, pinned, and texturing) FM layers contribute differently.

We confirm these expectations about the macroscopic AMR response of a single FM layer in different contact geometries by finite-element simulations using a commercial software.[22] In Fig. 4 we show the results for L and T geometry. The figure parts labeled "current" are the left and upper part of the current distribution in a rectangular sample in L and T geometry, respectively. The other halves of the sample follow from mirroring at the right and bottom edge, respectively. The gray levels indicate the local current density. The figure parts labeled "AMR" show the macroscopically measurable AMR ratio when one contact is fixed at the the position marked by a cross and the second contact is moved across the sample. Here, the gray levels render the macroscopically measured AMR ratio normalized the microscopic AMR ratio (note the different scale bars). In Fig. 4(a) the current distribution is more homogeneous and accordingly

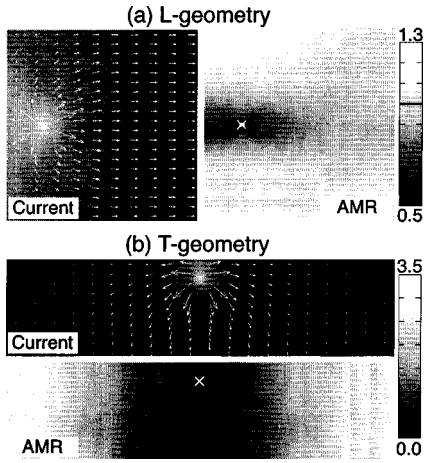

FIG. 4. Finite-element simulation for a rectangular sample contacted in (a) L geometry and (b) T geometry. The current distributions of (a) the left and (b) the upper half of the sample are shown. The other parts display the AMR measured when one contact is located at the position marked by a cross and the second contact is moved to different sites of the sample. The gray scales indicate the strength of the macroscopically measured AMR ratio divided by the microscopic AMR value.

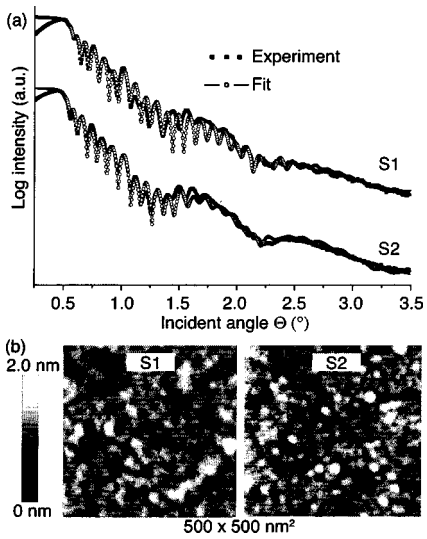

FIG. 5. (a) Specular XRR scans of sample S1 and S2. The curves are vertically shifted for the sake of clarity. (b) AFM micrographs of the completed spin-valves S1 and S2 taken under ambient conditions show similar surface roughness and average feature sizes.

the variations of the measured AMR are small. In the L geometry—the second contact lies on a horizontal line with the fixed contact—the macroscopic AMR approximately equals the microscopic. In Fig. 4(b) the current distribution is largely inhomogeneous and the measured AMR ratio is almost completely suppressed in some regions or strongly enhanced in others. In the T geometry with both contacts lying on a vertical line, the measured AMR ratio is only a few percent of the microscopic AMR ratio.

The possibility of strongly suppressing the AMR contribution to the angular MR is of particular interest because (i) a smaller number of parameters is required to fit Eq. (1) to the data, (ii) all AMR terms are suppressed simultaneously, (iii) the GMR term is not affected, and (iv) no information about the detailed remagnetization of additional and sometimes badly characterized FM layers (e.g., texturing layer) is needed.

V. RESULTS AND DISCUSSION

A. Structural characterization

It is well known that the GMR ratio depends on the state of the interface, i.e., on interface mixing and roughness ($\sigma_{\text{interface}}$).[23] Therefore, we start by characterizing the microstructural properties of the two types of samples. Figure 5(a) shows the XRR data of specimens S1 and S2. The specular reflectivity spectra are fitted using Parratt's formalism[24] with the following variables: the individual layer thicknesses and the average rms interface roughness $\sigma_{\text{interface}}$. We find that the layer thicknesses are the same for both samples and that there is no significant variation of $\sigma_{\text{interface}}=(0.5\pm0.05)$ nm. The diffuse scattering measurements provide information about the in-plane structure of the interfaces, which can be described in terms of the height-height correlation function $C(R)$. It is often parametrized in XDS analysis in the form

TABLE I. Average feature size and $\sigma_{surface}$ determined from AFM, GMR ratio, exchange bias field obtained from setup I (H_{EB}^{I}) and from setup II (H_{EB}^{II}), uniaxial anisotropy fields of the free ($Hu_f = Ku_f/M_f$) and pinned ($Hu_p = Ku_p/M_p$) FM layer, and interlayer coupling field ($H_J = J/\mu$) for samples S1 and S2.

	AFM		Setup I & II	Setup I	Setup II			
Sample	Feature size (nm)	$\sigma_{surface}$ (nm)	GMR (%)	H_{EB}^{I} (Oe)	H_{EB}^{II} (Oe)	Hu_p (Oe)	Hu_f (Oe)	H_J (Oe)
S1	32±5	0.36±0.05	1.8±0.05	147±20	150±5	3.3	4.1	5.1±1.0
S2	28±5	0.31±0.05	4.0±0.05	151±20	135±5	1.8	0.8	1.3±1.0

$$C(R) = \sigma_{interface}^2 \exp\left(-\left[\frac{|R|}{\xi}\right]^{2h}\right), \quad (2)$$

where **R** is an in-plane vector within the integration area, ξ is the in-plane correlation length, and h is the fractal dimension which describes the jaggedness of the interface.[18] We use Ming's model[25] to fit the XDS data (not shown) and obtain $\xi = (300 \pm 20)$ nm and $h = 0.5 \pm 0.2$. For details of the fitting procedure see Ref. 23. The fit results indicate no significant structural variation for the two sample types.

AFM micrographs in Fig. 5(b) show similar topographies irrespective of the difference in preparation. The small variation of the surface roughness $\sigma_{surface}$ and the average feature size determined from the AFM micrographs indicate a similar topological distribution of grains (see Table I). This is further supported by the volume-sensitive saturation resistances R_S, which are also the same for both sample types.

B. MOKE and MR measurements with setup I

Figure 6 shows the MOKE and MR measurements performed by varying the strength of the field applied collinear to the EBD (setup I). Both MOKE loops consist of two distinctly separate hysteresis loops corresponding to the free FM layer near zero field (small coercivity) and to the pinned FM layer (larger coercivity) centered at the exchange bias field of about 150 Oe. The hysteresis loop for the free layer of sample S1 is slightly narrower, probably due to the applied field of 130 Oe during the growth of this layer. The GMR ratio for S2 is almost twice as high as that of S1, although the structural parameters determined from XRR and AFM are almost the same (see Table I). The sizable error for H_{EB}^{I} arises from the sheared and asymmetric shape of the MOKE and MR loops of the pinned layer (see Fig. 6). The seemingly different shifts of the loops arise from the different responses of the MOKE and MR signal to the rotation of the pinned magnetization: A part of the sample, where the pinned magnetization, for instance, is perpendicular to the free magnetization does not contribute to the logitudinal MOKE loop, but shows a MR corresponding to 50% of the maximum GMR.

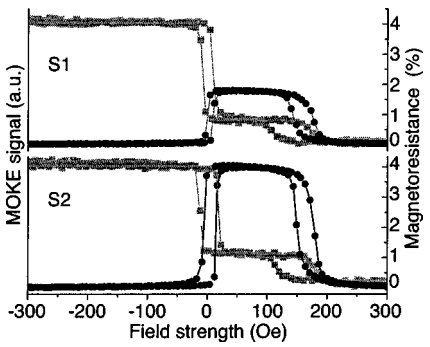

FIG. 6. Longitudinal MOKE hysteresis loops (gray) and MR curves (black) measured with setup I for spin-valves S1 and S2. MR measurements are performed in the L geometry.

C. MR measurements with setup II

Figure 7 shows the angular dependence of resistance R at different field strengths measured in the T geometry in order to experimentally suppress the AMR contributions. The external field is rotated starting from the EBD (corresponding to 0°) by 360° in clockwise (CW) direction and then back in counterclockwise (CCW) direction. The curves are dominated by the GMR effect and can be understood having in mind that parallel and antiparallel alignment between the pinned and free layers leads to a resistance minimum and maximum, respectively. At low fields (30–108 Oe) the magnetization of the pinned layer is approximately fixed in the EBD, while the free layer rotates with the field.

Therefore, the GMR effect leads to a sinusoidal shape of the curves. As the external field gets closer to the $|H_{EB}^{I}|$ of about 150 Oe (Table I) the deviation from the sinusoidal be-

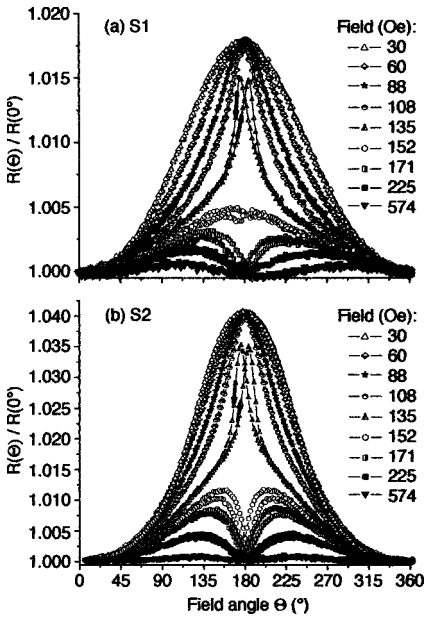

FIG. 7. Angular dependence of the resistance R for (a) S1 and (b) S2 normalized to the value for the EBD (corresponding to 0°) measured in T geometry at different external field strengths as indicated.

havior increases, and a difference between the CW and CCW rotation direction appears (see arrows in Fig. 7 for the curves at 135 Oe). As the field is increased above $|H_{EB}^{I}|$, the alignment between the magnetizations of the pinned and free layer at the field direction opposite to the EBD (180°) switches from antiparallel to parallel corresponding to a MR maximum and minimum, respectively. A further increase of the field strength leads to a gradually decreasing MR. Above 200 Oe, where the curves are dominated by the AMR effect, they become almost flat, because the impact of AMR on the angular MR is intentionally suppressed by choosing the T geometry. AMR in Fig. 7 is almost negligible compared to the GMR, and the AMR ratios extracted from the fits for both samples are less than 0.07%. Comparing the width of the angular MR curves of samples S1 and S2 one realizes a larger spread for S1. This signifies that for the two specimens the pinned and free layers respond differently to the external field due to different interlayer coupling strengths across the spacer layer.

We find rotational hysteresis in all examined samples in the field range around $|H_{EB}^{I}|$, where there is also hysteresis in the MR curves measured with setup I (Fig. 6). There are few reports of detailed studies of the rotational hysteresis examined by means of magnetic torque measurements[26,27] and in field-direction dependent MOKE (ROTMOKE) experiments.[28,29] Rotational hysteresis is a general but not yet completely understood feature of exchange-biased systems.

By simultaneously fitting the angular dependence of the MR at different field strengths to the model described in Sec. III, we are able to extract the strength H_{EB}^{II} and the direction of the exchange-bias fields, the uniaxial anisotropy fields $Hu_{f(p)}=Ku_{f(p)}/M_{f(p)}$ of the free (pinned) layer, and the interlayer coupling field $H_J=J/\mu$, where $M_{f,p}$ are the magnetizations of the free and pinned layer, and μ is the magnetic moment of the spin valve. For curves showing angular hysteresis we exclude the field region with a difference between the CW and CCW rotation directions from the fits. We also mention, that fitting of MR data taken in the L geometry is much more difficult and yields significantly larger error bars. In some cases no satisfactory fits are possible at all.

We find uniaxial anisotropy fields of 0.6%–3% of H_{EB}^{II} and weak ferromagnetic interlayer coupling with H_J about 4% of H_{EB}^{II} (see Table I). The collinearity of the uniaxial anisotropy axes and the EBD suggests that the uniaxial anisotropies are induced during the field-cooling procedure. Ferromagnetic coupling across thin spacers is quite common and can be attributed to "orange peel" coupling[30] due to finite interface roughness or to magnetic bridges.

The increase of the GMR ratio by more than a factor of 2 from S1 to S2 is accompanied by an almost fourfold decrease of H_J. Annealing of the complete structure for samples S2 obviously improves the interfaces in terms of roughness, which reduces the orange peel coupling as well as FM coupling due to magnetic bridges, and in terms of the maximum GMR ratio. The latter can be explained by a rearrangement of free magnetic poles at the Co/Cu interface[30] and also by the better interface quality. The uniaxial anisotropy fields extracted from the fits are slightly larger for S1

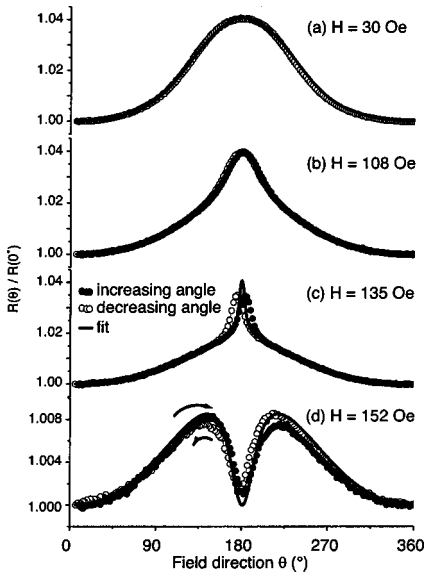

FIG. 8. Angular dependence of the resistance R in T geometry normalized to the value at 0° for sample S2 at different external field strengths (a) 30 Oe, (b) 108 Oe, (c) 135 Oe, and (d) 152 Oe. Filled and open circles are for the increasing (clockwise) and decreasing (counterclockwise) angular sweep, respectively. The solid lines show the fitted curves.

with a more pronounced difference for Hu_f of the free layer. The increased uniaxial anisotropy of the free layer arises from the applied field of 130 Oe during the growth of samples S1, but not for S2.

Comparing the values of H_{EB}^{I} and H_{EB}^{II} in Table I, one finds small differences within the error bars of H_{EB}^{I} and the significantly smaller error bars for H_{EB}^{II}. The reason for the smaller error bars—and the main advantage of setup II—is the fact that H_{EB}^{II} can be determined for external field strengths H clearly different from $|H_{EB}^{II}|$, where no domains and hysteresis occurs in the pinned layer. In setup I, however, H_{EB}^{I} is determined from the field where the remagnetization takes place and domains and hysteresis occur, i.e., at $H\approx -H_{EB}^{I}$.

Figure 8 shows representative examples of fits for some experimental curves from Fig. 7(b). The deviations of the model from the data in Figs. 8(c) and 8(d) are due to hysteresis and suggest the following remagnetization behavior: when coming from the EBD ($\theta=0°$), the magnetization of pinned layer rotates coherently until θ reaches a critical value of about 10° before the inverse EBD, $\theta=170°$. At this point domains begin to nucleate, and the GMR ratio—compared to the single-domain state of the model—is reduced for $H<H_{EB}^{II}$ [Fig. 8(c)] and enhanced for $H>H_{EB}^{II}$ [Fig. 8(d)]. From here the reversal continues via domain wall motion up to about 15° and 70° beyond the inverse EBD ($\theta=195°$ and 250°) for $H=135$ and 152 Oe, respectively. Thus, there is a difference of 55° before the single-domain state is restored for $H<H_{EB}^{II}$ and $H>H_{EB}^{II}$. This kind of angular hysteresis for different external fields has previously been reported for torque measurements.[27] Otherwise, we find symmetric CW and CCW curves around 180° unlike those reported by de Haas *et al.*[28] This symmetry confirms for our samples that there is no misalignment between the uniaxial and unidirec-

tional anisotropy axes. We also do not observe a distinct distribution of EBDs as alluded to by Barholz and Mattheis.[31]

VI. CONCLUSIONS

We have described in detail angular MR measurements of exchange-biased spin valves. We showed experimentally and by finite-element simulations that AMR contributions can be suppressed by choosing an appropriate contact geometry. The advantage of varying the field direction (setup II) over standard MOKE and MR loops with fixed field direction (setup I) is the higher accuracy in determining the GMR ratio, the uniaxial anisotropies of the free and pinned FM layers, and the interlayer coupling between them. The higher precision results from (i) the intrinsically larger data set (variation of field magnitude *and* direction), and (ii)—in particular for H_{EB}—from the fact that the measurements can be performed at external fields smaller or larger than H_{EB}, where no hysteresis and domains are involved. The application to differently prepared Ta(5.0 nm)/NiFe(3.0 nm)/FeMn(15.5 nm)/NiFe(3.0 nm)/Co(2.0 nm) / Cu(3.5 nm)/Co(2.0 nm)/NiFe(7.0 nm) spin valves demonstrates the high sensitivity and reveals small differences of the anisotropy and interlayer coupling fields, which are hardly accessible by standard MR and MOKE loops. The described procedures allow for a quick and precise characterization of unpatterned spin-wave multilayer stacks.

[1]B. Dieny, J. Magn. Magn. Mater. **136**, 335 (1994).
[2]W. H. Meiklejohn and C. P. Bean, Phys. Rev. **102**, 1413 (1956).
[3]J. Nogués and I. K. Schuller, J. Magn. Magn. Mater. **192**, 203 (1999).
[4]A. E. Berkowitz and K. Takano, J. Magn. Magn. Mater. **200**, 552 (1999).
[5]G. Binasch, P. Grünberg, F. Saurenbach, and W. Zinn, Phys. Rev. B **39**, 4828 (1989).
[6]M. N. Baibich, J. M. Broto, A. Fert, F. Nguyen Van Dau, F. Petroff, P. Etienne, G. Creuzet, A. Friedrich, and J. Chazelas, Phys. Rev. Lett. **61**, 2472 (1988).
[7]B. H. Miller and E. D. Dahlberg, Appl. Phys. Lett. **69**, 3932 (1996).
[8]K.-U. Barholz and R. Mattheis, J. Appl. Phys. **91**, 7224 (2002).
[9]R. H. Norton, IEEE Trans. Magn. **19**, 1579 (1983).
[10]T. C. Huang, J.-P. Nozieres, V. S. Speriosu, B. A. Gurney, and H. Lefakis, Appl. Phys. Lett. **62**, 1478 (1993).
[11]K. Nishioka, C. Hou, H. Fujiwara, and R. D. Metzger, J. Appl. Phys. **80**, 4528 (1996).
[12]G. Choe and S. Gupta, Appl. Phys. Lett. **70**, 1766 (1997).
[13]M. Konoto, M. Tsunda, and M. Takahashi, J. Appl. Phys. **85**, 4925 (1999).
[14]M. Mao, C. Cerjan, B. Law, F. Grabner, and S. Vaidya, J. Appl. Phys. **87**, 4933 (2000).
[15]R. Meservy and P. M. Tedrow, Phys. Rep. **238**, 173 (1994).
[16]Th. G. S. M. Rijks, R. Coehoorn, M. J. M. de Jong, and W. J. M. de Jonge, Phys. Rev. B **51**, 283 (1995).
[17]B. H. Miller, E. Y. Chen, and E. D. Dahlberg, J. Appl. Phys. **73**, 6384 (1993).
[18]T. Salditt, T. H. Metzger, and J. Peisl, Phys. Rev. Lett. **73**, 2228 (1994).
[19]A. Paul and G. S. Lodha, Phys. Rev. B **65**, 245416 (2002).
[20]M. Buchmeier, B. K. Kuanr, R. R. Gareev, D. E. Bürgler, and P. Grünberg, Phys. Rev. B **67**, 184404 (2003).
[21]H. A. M. van den Berg, W. Clemens, G. Gieres, G. Rupp, W. Schelter, and M. Vieth, IEEE Trans. Magn. **32**, 4624 (1996).
[22]FEMLAB®, COMSOL AB, Sweden 1994–2000.
[23]A. Paul, J. Magn. Magn. Mater. **240**, 497 (2002).
[24]L. G. Parratt, Phys. Rev. **95**, 359 (1954).
[25]Z. H. Ming, A. Krol, Y. L. Soo, Y. H. Kao, J. S. Park, and K. L. Wang, Phys. Rev. B **47**, 16373 (1993).
[26]K. Zhang, T. Kai, T. Zhao, H. Fujiwara, C. Hou, and M. T. Kief, J. Appl. Phys. **89**, 7546 (2001).
[27]M. Tsunoda, Y. Tsuchiya, T. Hashimoto, and M. Takahashi, J. Appl. Phys. **87**, 4375 (2000).
[28]O. de Haas, R. Schäfer, L. Schultz, K.-U. Barholz, and R. Mattheis, J. Magn. Magn. Mater. **260**, 380 (2003).
[29]D. Tietjen, D. Elefant, and C. M. Schneider, J. Appl. Phys. **91**, 5951 (2002).
[30]A. Paul, T. Damm, D. E. Bürgler, H. Kohlstedt, S. Stein, and P. Grünberg, J. Phys.: Condens. Matter **15**, 2471 (2003).
[31]K.-U. Barholz and R. Mattheis, IEEE Trans. Magn. **38**, 2767 (2002).